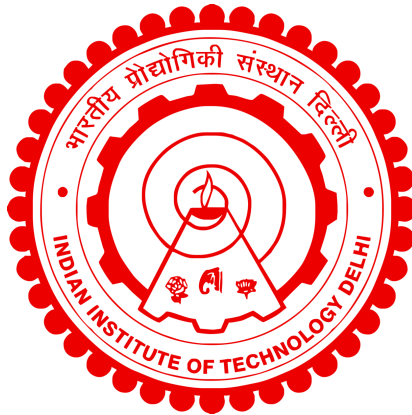


THERMOCAPILLARY INSTABILITY OF FILM FLOWS

ARNAB CHOUDHURY



DEPARTMENT OF APPLIED MECHANICS

INDIAN INSTITUTE OF TECHNOLOGY DELHI

DECEMBER 2024

© Indian Institute of Technology Delhi (IITD), New Delhi, 2024

THERMOCAPILLARY INSTABILITY OF FILM FLOWS

by

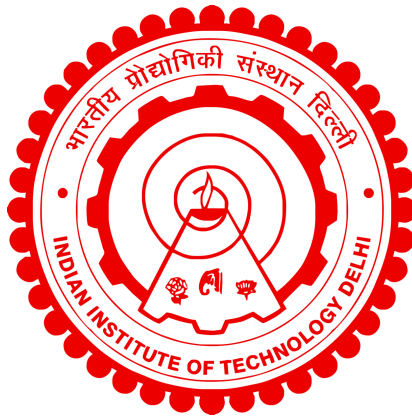
ARNAB CHOUDHURY

Department of Applied Mechanics

Submitted

in fulfillment of the requirements of the degree of Doctor of Philosophy

to the



INDIAN INSTITUTE OF TECHNOLOGY DELHI

December 2024

Certificate

This is to certify that the thesis **Mr. Arnab Choudhury** submitted for consideration for the degree of Doctor of Philosophy at the Indian Institute of Technology Delhi, entitled “**Thermocapillary instability of film flows**” is an accurate account of the legitimate research work he conducted under my direction and supervision. I believe that the thesis is deserving of consideration for the degree of Doctor of Philosophy under the institute regulations as **Mr. Arnab Choudhury** has complied with all the necessary prerequisites. The contents of this thesis have not been submitted in whole or in part to any other college or institute for the granting of any degree or diploma.

Dr. Arghya Samanta

Associate Professor
Department of Applied Mechanics
Indian Institute of Technology Delhi
New Delhi-110016
India

Place: New Delhi
Date : 20/12/2024

Acknowledgements

Ph.D. is more than just a degree; it is a journey of curiosity, perseverance, and growth for those who dream of researching the intricate and fascinating complexities of nature, industry, and society. Throughout my Ph.D. journey, I have encountered both easy and challenging times, which I thoroughly enjoyed. As I reflect on this transformative experience, I am deeply indebted to many individuals whose support made this journey possible.

First and foremost, I would like to express my heartfelt gratitude to my supervisor, Dr. Arghya Samanta, for his constant guidance, wisdom, and unwavering support. Whenever I faced difficulties, I could always approach him for discussion, and he was available most of the time in his office or over a phone call. I have always admired his hardworking abilities and dedication to research, which has deeply inspired me as a Ph.D. student. I must admit that without his support and suggestions, completing this work would have taken much longer.

My sincere appreciation goes to my Student Research Committee members: Dr. S. V. Veeravalli, Dr. V. K. Chalamalla, and Dr. S. Dutta, for their valuable suggestions and constructive feedback, which have significantly enhanced the quality of this thesis. Their expertise and guidance were immensely helpful throughout this process.

A special mention goes to all my friends, lab mates, and colleagues, whose support, lively discussions, and companionship made this journey more enjoyable. Their friendship has been a constant source of motivation.

I am deeply grateful to my family for their unconditional love, encouragement, and patience throughout these years. Their belief in me and constant support kept me going during the most challenging times and helped me stay focused on my research work.

Finally, I acknowledge the financial support provided by Govt. of India and the Indian Institute of Technology Delhi, which made this research possible. I am also thankful to all those, both near and far, who contributed in any way to the successful completion of this work.

Arnab Choudhury

Abstract

The study of interfacial heat transfer and the stability of thin liquid films has garnered significant attention from researchers worldwide, owing to their broad applications in both engineering and science. Thin liquid films are frequently encountered in various industrial equipment, such as falling film evaporators and crystallizers, due to their extensive contact area and minimal thermal resistance. Moreover, the formation of solitary waves on the surface of these films considerably enhance heat and mass transfer rates. Thin liquid films are also employed for cooling micro-electronic devices and providing thermal protection for rocket engines. Beyond their engineering significance, the study of heated falling films is also relevant from a fundamental standpoint in heat transfer and fluid mechanics, where surface heat transfer plays a key role in shaping the surface wave dynamics under the influence of gravity. In this thesis, we tried to investigate the linear stability of a heated thin liquid film flow under different conditions. In particular, the motivation is to investigate the thermocapillary instability in the presence of insoluble surfactant and applied shear stress.

In the first study, a linear stability analysis of a three-dimensional thin liquid film flowing down a uniformly heated slippery inclined plane is carried out for disturbances of arbitrary wavenumbers, where the liquid film satisfies Newton's law of cooling at the film surface. A coupled system of boundary value problems is formulated in terms of the amplitudes of perturbation normal velocity and perturbation temperature, respectively. Analytical solution of the boundary value problems demonstrates the existence of three dominant modes, the so-called H-mode (surface mode), S-mode, and P-mode, where the S-mode and P-mode emerge due to the thermocapillary effect. In particular, the H-mode appears due to the stream-wise component of the gravitational force, whereas the shear mode arises due to the viscous effect when the Reynolds number is very high, but the inclination angle is sufficiently small. It is found that the onset of instabilities for the H-mode, S-mode, and P-mode reduce in the presence of wall slip and leads to a destabilizing influence. Numerical solution based on the Chebyshev spectral collocation method unveils that the finite wavenumber H-mode instability can be stabilized, but the S-mode instability and the finite wavenumber P-mode instability can be destabilized

by increasing the value of the thermal Marangoni number. On the other hand, the Biot number shows a dual role in the H-mode and S-mode instabilities. But the P-mode instability can be made stable with the increasing value of the Biot number and the decreasing values of the thermal Marangoni number and the Prandtl number. Furthermore, the H-mode and S-mode instabilities become weaker, but the P-mode instability becomes stronger with the increasing value of the spanwise wavenumber. In addition, the shear mode emerges in the numerical simulation when the Reynolds number is large, which can be destabilized slightly with the increasing value of the thermal Marangoni number; however, it can be stabilized with the increasing value of the slip length and introducing the spanwise wavenumber to the infinitesimal perturbation. The current results also report that Squire's statement holds for the H-mode and the shear mode.

In the second study, we investigate the linear stability analysis of a gravity-driven three-dimensional incompressible viscous fluid flowing down a uniformly heated inclined plane under the influence of an external constant shear stress on the fluid surface. Based on a coupled system of boundary value problems involving the amplitudes of the perturbation normal velocity and perturbation temperature, the stability analysis is accomplished for infinitesimal disturbances of arbitrary wavenumbers. The analytical solution of the boundary value problems in the long-wave regime reveals the existence of the H-mode, which is destabilized by both the thermal Marangoni number and the imposed shear stress acting in the co-flow direction. Furthermore, we determine the critical value of the thermal Marangoni number below which the inertialess flow is linearly stable, but the flow may be linearly unstable in this range due to inertia. On the other hand, the numerical solution based on the Chebyshev spectral collocation method reveals that the H-mode and S-mode instabilities are destabilized, but the P-mode instability is stabilized if the constant shear stress is applied in the co-flow direction. Interestingly, as the imposed shear stress rises, the onset of instability for the H-mode and the onset of stability for the S-mode merge with each other and produce a single onset for the primary stability. However, a completely opposite phenomenon takes place if a constant shear stress is imposed in the counter-flow direction. In addition, we observe that the shear mode instability can be initiated at a lower Reynolds number by applying a constant shear stress in the co-flow direction. Conversely, the shear mode instability can be delayed by imposing a constant shear stress in the counter-flow direction.

In the third and final study, we examine the linear thermocapillary instability of a two-dimensional gravity-driven shear-imposed incompressible viscous film flowing over a uniformly heated inclined wall when the film surface is covered by an insoluble surfactant. The aim is to expand the prior research [H. H. Wei, “Effect of surfactant on the long-wave instability of a shear-imposed liquid flow down an inclined plane,” *Phys. Fluids* 17, 012103 (2005)] to the case of a non-isothermal viscous film. As a result, the energy equation and the surfactant transport equation are incorporated into the governing equations along with the mass conservation and momentum equations. The long-wave analysis predicts that the surfactant Marangoni number has a stabilizing impact on the H-mode, but the thermal Marangoni number has a destabilizing impact. These opposing effects produce an analytical relationship between them for which the critical Reynolds number for the H-mode instability of the non-isothermal film flow coincides with that of the isothermal film flow. On the other hand, the numerical result exhibits that the surfactant Marangoni number has a stabilizing influence on the thermocapillary S-mode and P-mode. More specifically, these thermocapillary instabilities diminish with an increase in the value of the surfactant Marangoni number. However, these thermocapillary instabilities can be made stronger by increasing the value of the thermal Marangoni number. Furthermore, the thermal Marangoni number destabilizes the surfactant mode instability, but the onset of instability is not affected in the presence of the thermal Marangoni number, which is in contrast to the influence of the surfactant Marangoni number on the onset of surfactant mode instability. Interestingly, the Biot number shows a dual role in the surfactant mode instability, even though the threshold of instability remains the same. The shear mode instability is stabilized by the surfactant Marangoni number but destabilized by the thermal Marangoni number. Moreover, the comparison of results with inertia and without inertia exhibits a stabilizing role of inertia in the surfactant mode.

सारांश

अंतरापृष्ठीय ऊष्मा स्थानांतरण और पतली तरल फिल्मों की स्थिरता के अध्ययन ने दुनिया भर के शोधकर्ताओं का ध्यान आकर्षित किया है, क्योंकि अभियांत्रिकी और विज्ञान दोनों में उनके व्यापक अनुप्रयोग हैं। पतली तरल फिल्मों अपने बड़े संपर्क क्षेत्र और कम तापीय प्रतिरोध के कारण गिरती हुई फिल्म वाष्पीकरणकर्ताओं और क्रिस्टलाइज़रों जैसे औद्योगिक उपकरणों में उपयोग होती हैं। इसके अलावा, इन फिल्मों की सतह पर एकल (सॉलिडरी) लहरों का निर्माण ऊष्मा और द्रव्यमान स्थानांतरण दरों को काफी हद तक बढ़ाता है। पतली तरल फिल्मों का उपयोग सूक्ष्म-इलेक्ट्रॉनिक उपकरणों को ठंडा करने और रॉकेट इंजनों के लिए तापीय सुरक्षा प्रदान करने के लिए भी किया जाता है। तापित गिरती फिल्मों का अध्ययन न केवल उनके अभियांत्रिकी महत्व के लिए, बल्कि ऊष्मा स्थानांतरण और द्रव यांत्रिकी के मौलिक दृष्टिकोण से भी प्रासंगिक है, जहां सतही ऊष्मा स्थानांतरण गुरुत्वाकर्षण के प्रभाव से सतही तरंगों की गतिशीलता को आकार देने में अहम भूमिका निभाता है। इस थीसिस में, हमने विभिन्न स्थितियों के तहत एक तापित पतली तरल फिल्म प्रवाह की रैखिक स्थिरता की जांच करने की कोशिश की है। विशेष रूप से, प्रेरणा यह है कि अधुलनशील सर्फेक्टेंट और लगाए गए अपरूपण तनाव की उपस्थिति में थर्मोकैपिलरी अस्थिरता की जांच की जाए।

पहले अध्ययन में, एक समान रूप से तापित फिसलन भरे झुके हुए तल पर प्रवाहित हो रही तीन-आयामी पतली तरल फिल्म की रेखीय स्थिरता विश्लेषण किया गया है, जिसमें किसी भी तरंग संख्या वाले विचलनों को शामिल किया गया है। इस दौरान तरल फिल्म सतह पर न्यूटन के शीतलन नियम का पालन करती है। सीमा मूल्य समस्याओं की एक युग्मित प्रणाली को विचलन लम्बवत वेग और विचलन तापमान के आयामों के संदर्भ में तैयार किया गया है। सीमा मूल्य समस्याओं का विश्लेषणात्मक समाधान तीन प्रमुख मोडों के अस्तित्व को प्रदर्शित करता है, तथाकथित एच-मोड (सतह मोड), एस-मोड और पी-मोड, जहां एस-मोड और पी-मोड थर्मोकैपिलरी प्रभाव के कारण उभरते हैं। विशेष रूप से, एच-मोड गुरुत्वाकर्षण बल के प्रवाहीय घटक के कारण प्रकट होता है। जब रेनॉल्ड्स संख्या बहुत अधिक होती है लेकिन झुकाव का कोण पर्याप्त रूप से छोटा होता है, तब शियर मोड श्यान प्रभाव के कारण उत्पन्न होता है। यह पाया गया है कि एच-मोड, एस-मोड और पी-मोड के लिए अस्थिरताओं की शुरुआत फिसलन की उपस्थिति में कम हो जाती है और यह अस्थिर प्रभाव को बढ़ावा देती है। चेबीशेव स्पेक्ट्रल कोलोकेशन विधि पर आधारित संख्यात्मक समाधान से पता चलता है कि थर्मल मैरंगोनी संख्या के मूल्य को बढ़ाकर परिमित तरंग संख्या एच-मोड अस्थिरता को स्थिरता प्रदान किया जा सकता है, लेकिन एस-मोड अस्थिरता और परिमित तरंग संख्या पी-मोड अस्थिरता को और अस्थिर किया जा सकता है। दूसरी ओर, बायोट संख्या एच-मोड और एस-मोड अस्थिरता में दोहरी भूमिका दिखाती है। लेकिन बायोट संख्या के बढ़ते मूल्य और थर्मल मैरंगोनी संख्या और प्रांटल संख्या के घटते मूल्यों के साथ पी-मोड अस्थिरता को स्थिर बनाया जा सकता है। इसके अलावा, अनुप्रस्थ तरंग संख्या के मान में वृद्धि के साथ, एच-मोड और एस-मोड अस्थिरताएँ घटने लगती हैं, लेकिन पी-मोड अस्थिरता बढ़ने लगती है। इसके अलावा, संख्यात्मक सिमुलेशन में शियर मोड तब उभरता

है जब रेनॉल्ड्स संख्या अधिक होती है। इसे थर्मल मारंगोनी संख्या के मान में वृद्धि से थोड़ा और अस्थिर किया जा सकता है; हालांकि, इसे फिसलन लंबाई के मान में वृद्धि और अनुप्रस्थ तरंग संख्या को सूक्ष्म विचलन में शामिल करके स्थिर किया जा सकता है। वर्तमान परिणाम यह भी बताते हैं कि स्क्वायर का कथन एच-मोड और शियर मोड के लिए मान्य है।

दूसरे अध्ययन में, हमने एक समान रूप से तापित झुके हुए तल पर प्रवाहित हो रहे गुरुत्वाकर्षण-प्रेरित तीन-आयामी असंपीड्य श्यान तरल की रेखीय स्थिरता का विश्लेषण किया है, जिसमें तरल की सतह पर बाहरी स्थिर अपरूपण तनाव का प्रभाव शामिल है। विचलन लम्बवत वेग और विचलन तापमान के आयामों से संबंधित सीमा मान समस्याओं की एक युग्मित प्रणाली के आधार पर, किसी भी तरंग संख्या वाले सूक्ष्म विचलनों के लिए स्थिरता विश्लेषण किया गया है। लंबी-तरंग क्षेत्र में सीमा मान समस्याओं के विश्लेषणात्मक समाधान से एच-मोड की उपस्थिति का पता चलता है, जिसे थर्मल मारंगोनी संख्या और सह-प्रवाह दिशा में कार्य करने वाले लगाए गए अपरूपण तनाव दोनों के द्वारा अस्थिर किया जा सकता है। इसके अलावा, हम थर्मल मारंगोनी संख्या का वह क्रांतिक मान निर्धारित करते हैं जिसके नीचे अ-जड़त्वीय प्रवाह रैखिक रूप से स्थिर रहता है, लेकिन इस सीमा के भीतर जड़त्व के कारण प्रवाह रैखिक रूप से अस्थिर हो सकता है। दूसरी ओर, चेबिшев स्पेक्ट्रल कोलोकेशन विधि पर आधारित संख्यात्मक समाधान से पता चलता है कि यदि सह-प्रवाह दिशा में स्थिर अपरूपण तनाव लागू किया जाए, तो एच-मोड और एस-मोड अस्थिरताएँ और अस्थिर हो जाती हैं, लेकिन पी-मोड अस्थिरता स्थिर होने की कोशिश करती है। दिलचस्प रूप से, जैसे-जैसे लगाए गए अपरूपण तनाव में वृद्धि होती है, एच-मोड के लिए अस्थिरता की शुरुआत और एस-मोड के लिए स्थिरता की शुरुआत आपस में मिल जाती हैं और प्राथमिक स्थिरता के लिए एक ही शुरुआत उत्पन्न करती हैं। हालांकि, यदि विपरीत प्रवाह दिशा में स्थिर अपरूपण तनाव लागू किया जाए, तो एक बिल्कुल विपरीत घटना होती है। इसके अतिरिक्त, हम देखते हैं कि शियर मोड अस्थिरता को सह-प्रवाह दिशा में स्थिर अपरूपण तनाव लागू करके कम रेनॉल्ड्स संख्या पर भी आरंभ किया जा सकता है। इसके विपरीत, विपरीत प्रवाह दिशा में स्थिर अपरूपण तनाव लागू करके शियर मोड अस्थिरता को विलंबित किया जा सकता है।

तीसरे और अंतिम अध्ययन में, हम एक दो-आयामी गुरुत्व-प्रेरित अपरूपण लागू असंपीड्य श्यान फिल्म की रेखीय थर्मोकैपिलरी अस्थिरता की जांच करते हैं, जो एक समान रूप से ऊष्म झुकी हुई सतह पर प्रवाहित हो रही है और जिसकी सतह पर अधुलनशील सर्फैक्टेंट मौजूद है। इसका उद्देश्य पिछले शोध [एच. एच. वेई, "Effect of surfactant on the long-wave instability of a shear-imposed liquid flow down an inclined plane," फिज. फ्लूइड्स १७, ०१२१०३ (२००५)] को एक गैर-साम्य तापीय श्यान फिल्म के संदर्भ में विस्तारित करना है। परिणामस्वरूप, ऊर्जा समीकरण और सर्फैक्टेंट परिवहन समीकरण को द्रव्यमान संरक्षण और संवेग समीकरणों के साथ संचालन समीकरणों में सम्मिलित किया गया है। लंबी-तरंग विश्लेषण यह संकेत देता है कि सर्फैक्टेंट मारंगोनी संख्या का एच-मोड पर स्थिरकारी प्रभाव पड़ता है, जबकि थर्मल मारंगोनी संख्या का अस्थिरकारी प्रभाव होता है। ये विपरीत प्रभाव उनके बीच एक विश्लेषणात्मक संबंध स्थापित करते हैं, जिसके परिणामस्वरूप गैर-साम्य तापीय फिल्म प्रवाह

की एच-मोड अस्थिरता के लिए क्रांतिक रेनॉल्ड्स संख्या साम्य तापीय फिल्म प्रवाह की क्रांतिक रेनॉल्ड्स संख्या से मेल खाती है। दूसरी ओर, संख्यात्मक परिणाम यह दर्शाता है कि सर्फेक्टेंट मारंगोनी संख्या का थर्मोकैपिलरी एस-मोड और पी-मोड पर स्थिरकारी प्रभाव होता है। और अधिक विशिष्ट रूप से, इन थर्मोकैपिलरी अस्थिरताएँ सर्फेक्टेंट मारंगोनी संख्या के मान में वृद्धि के साथ कम हो जाती हैं। हालांकि, इन थर्मोकैपिलरी अस्थिरताओं को थर्मल मारंगोनी संख्या के मान में वृद्धि करके और अधिक अस्थिर बनाया जा सकता है। इसके अतिरिक्त, थर्मल मारंगोनी संख्या सर्फेक्टेंट मोड अस्थिरता को और अस्थिर करती है, लेकिन थर्मल मारंगोनी संख्या की उपस्थिति में अस्थिरता की शुरुआत पर कोई प्रभाव नहीं पड़ता, जो सर्फेक्टेंट मोड अस्थिरता की शुरुआत पर सर्फेक्टेंट मारंगोनी संख्या के प्रभाव के विपरीत है। दिलचस्प रूप से, बायोट संख्या सर्फेक्टेंट मोड अस्थिरता में दोहरी भूमिका निभाती है, हालांकि अस्थिरता की सीमा वही रहती है। सर्फेक्टेंट मारंगोनी संख्या शियर मोड अस्थिरता को स्थिरता प्रदान करती है, लेकिन थर्मल मारंगोनी संख्या इसे और अस्थिर करती है। इसके अलावा, जड़त्व के साथ और जड़त्व के बिना प्राप्त परिणामों की तुलना सर्फेक्टेंट मोड में जड़त्व की स्थिरकारी भूमिका को दर्शाती है।

Contents

Certificate	i
Acknowledgements	ii
Abstract	iv
Contents	x
List of Figures	xv
List of Tables	xxi
Symbols	xxiii
1 Introduction	1
1.1 Hydrodynamic Stability	3
1.2 Literature Survey	4
1.3 Applications	12
1.4 Objectives	12
1.4.1 Objective 1	13
1.4.2 Objective 2	14
1.4.3 Objective 3	14
1.5 Organization of the Thesis	15
2 Methodologies	17
2.1 Introduction	17
2.2 Governing Equations	17
2.3 Boundary Conditions	18
2.3.1 Boundary conditions at the inclined plane	19
2.3.2 Boundary conditions at the free surface	19
2.4 Orr-Sommerfeld Type Boundary Value Problem (OS-BVP)	22

2.5	Solution Procedures	24
2.5.1	Long-wave analysis	24
2.5.2	Padé approximation	25
2.5.3	Arbitrary wavenumber analysis	25
2.5.4	Inertialess Analysis	27
3	Linear stability of a falling film down a heated slippery plane	29
3.1	Introduction	29
3.2	Mathematical Formulation	30
3.2.1	Governing equations & boundary conditions	31
3.2.2	Non-dimensionalization	33
3.2.3	Perturbation equations	35
3.2.4	Orr-Sommerfeld type boundary value problem	37
3.3	Analytical solution of the boundary value problem	38
3.3.1	Streamwise perturbation in the long-wave regime	38
3.3.2	Zeroth-order approximation	39
3.3.3	First-order approximation	40
3.3.4	Second-order approximation	43
3.3.5	Spanwise perturbation in the arbitrary wavenumber regime	45
3.4	Numerical solution of the boundary value problem	48
3.4.1	Validation of the numerical code	50
3.4.2	Effect of the thermal Marangoni number	53
3.4.3	Effect of the Biot number	58
3.4.4	Effect of the slip length	63
3.4.5	Effect of the Prandtl number	68
3.4.6	Effect of the spanwise wavenumber	69
4	Linear stability of a shear-imposed heated falling film	73
4.1	Introduction	73
4.2	Mathematical Formulation	74
4.2.1	Governing equations & boundary conditions	75
4.2.2	Non-dimensionalization	77
4.2.3	Perturbation equations	80
4.2.4	Orr-Sommerfeld-type boundary value problem	81
4.3	Analytical solution of the Orr-Sommerfeld-type boundary value problem	83
4.3.1	Long-wave solution	83
4.3.2	Zeroth-order approximation	84
4.3.3	First-order approximation	85
4.3.4	Second-order approximation	89
4.3.5	Third-order approximation	89

4.4	Numerical solution of the Orr-Sommerfeld-type boundary value problem	91
4.4.1	Validation of the numerical code	93
4.4.2	Convergence of the spectrum	96
4.5	Results in low to moderate Reynolds number regime	99
4.5.1	Effect of the imposed shear stress	99
4.5.2	Effect of the spanwise wavenumber	103
4.6	Results in high Reynolds number regime	104
4.7	Inertialess stability analysis	108
4.8	Inviscid stability analysis	112
4.9	Relation to the spreading problem where the liquid front propagates in the flow direction	115
5	Linear stability of a contaminated shear-imposed heated falling film	121
5.1	Introduction	121
5.2	Mathematical Formulation	122
5.2.1	Governing equations & boundary conditions	123
5.2.2	Non-dimensionalization	125
5.2.3	Perturbation equations	127
5.3	Orr-Sommerfeld-type equation	128
5.3.1	Long-wave analytical solution of the Orr-Sommerfeld-type equation	130
5.3.2	Zeroth-order approximation	131
5.3.3	First-order approximation	132
5.3.4	Second-order approximation	139
5.3.5	Third-order approximation	139
5.4	Numerical solution of the Orr-Sommerfeld-type equation	143
5.4.1	Effects of the surfactant Marangoni number and the thermal Marangoni number on the H-mode, S-mode, and P-mode in the low to moderate Reynolds number regime.	149
5.4.2	Effects of the thermal Marangoni number, the surfactant Marangoni number, and the Biot number on the surfactant mode	152
5.4.3	Effects of the surfactant Marangoni number and the thermal Marangoni number on the shear mode	156
5.5	Inertialess stability analysis	157
6	Conclusion	163
6.1	Introduction	163
6.2	Summary of the Present Work	164
6.2.1	Linear stability of a falling film down heated slippery plane	164
6.2.2	Linear stability of a shear-imposed heated falling film	167

6.2.3	Linear stability of a contaminated shear-imposed heated falling film	169
6.3	Scope of Future Work	172
A	Squire’s transformation for non-isothermal flow configuration	173
B	Long wave expressions and coefficients	177
B.1	Expressions and coefficients in <i>Chapter 3</i>	177
B.1.1	Solution of first order long-wave equations	177
B.1.2	Expressions of the coefficients for c_3	178
B.2	Expressions and coefficients in <i>Chapter 4</i>	179
B.2.1	Solution of the first-order long-wave equations	179
B.2.2	Long-wave second-order approximation	180
B.2.3	Expressions of the coefficients for c_3	180
B.3	Expressions and coefficients in <i>Chapter 5</i>	181
B.3.1	Coefficients of $\phi_1(y)$ and $T_1(y)$	181
B.3.2	Coefficients of c_{1s} and Γ_1	182
B.3.3	Coefficients of c_{2s} and c_{2m}	182
B.3.4	Coefficients of c_{3s} and c_{3m}	183
B.3.5	Coefficients of c_{3s} and c_{3m} for inertialess flow	184
	Bibliography	185
	List of Publications	195
	Author Bio-Data	197

List of Figures

1.1	Unstable waves on the surface of water flowing down a slightly inclined plane.	2
1.2	Falling film crystallizer.	13
2.1	Sketch of a heated liquid film flowing down an inclined plane.	18
2.2	Three-dimensional geometry of the free surface of a thin liquid film.	19
3.1	Schematic diagram of a thin liquid film flowing down a heated slippery inclined plane.	30
3.2	(a) Variation of the critical Reynolds number Re_c with the thermal Marangoni number Ma_T for the H-mode when the slip length β varies. (b) Comparison of temporal growth rate for the H-mode with the results obtained from the Padé approximation and numerical solution.	43
3.3	(a) Neutral stability curve for the stationary instability in (k_z, Ma_T^*) plane when $k_x = 0$. The diamond points are the results of Kalliadasis <i>et al.</i> (b) Neutral stability curve for the stationary instability in (k_z, Ma_T^*) plane for different values of k_x . The circular points represent the analytical result when $k_x = 0$	47
3.4	(a) Variation of the temporal growth rate ω_i for the H-mode with streamwise wavenumber k_x for different values of M_T . The symbolic points are the results of Ding <i>et al.</i> (b) Variation of the neutral stability curves in (Re, k_x) plane for different values of M_T . The symbolic points are the results of Kalliadasis <i>et al.</i>	50
3.5	(a)-(d) The eigenvalues in (c_r, c_i) plane for different unstable modes of instability.	53
3.6	(a) Variation of the neutral stability curve for the H-mode in (Re, k_x) plane for different values of M_T . (b) Variation of the temporal growth rate ω_i for the H-mode with streamwise wavenumber k_x for different values of M_T when $Re = 5$ (top) and $Re = 40$ (bottom).	54

3.7	(a) Variation of the neutral stability curve for the thermocapillary S-mode in (Re, k_x) plane for different values of M_T . (b) Variation of the temporal growth rate ω_i for the thermocapillary S-mode with streamwise wavenumber k_x for different values of M_T (top). Variation of the phase speed c_r for the thermocapillary S-mode with streamwise wavenumber k_x for different values of M_T (bottom).	55
3.8	(a) Variation of the neutral stability curve for the thermocapillary P-mode in (Re, k_x) plane for different values of M_T . (b) Variation of the temporal growth rate ω_i for the thermocapillary P-mode with streamwise wavenumber k_x for different values of M_T (top). Variation of the phase speed c_r for the thermocapillary P-mode with streamwise wavenumber k_x for different values of M_T when (bottom).	57
3.9	(a) Variation of the neutral stability curve for the shear mode in (Re, k_x) plane for different values of the thermal Marangoni number Ma_T . (b) Variation of the temporal growth rate ω_i for the shear mode with streamwise wavenumber k_x for different values of Ma_T	58
3.10	(a) Variation of the neutral stability curve for the H-mode and S-mode in (Re, k_x) plane for different values of B ($B \leq 0.5$). (b) Variation of the neutral stability curve for the H-mode and S-mode in (Re, k_x) plane for different values of B ($B \geq 1$).	59
3.11	(a) Variation of the temporal growth rate ω_i for the H-mode with streamwise wavenumber k_x for different values of B ($B \leq 0.5$) when $Re = 5$ (top) and $Re = 20$ (bottom). (b) Variation of the temporal growth rate ω_i for the H-mode with streamwise wavenumber k_x for different values of B ($B \geq 1$) when $Re = 5$ (top) and $Re = 20$ (bottom).	60
3.12	(a) Variation of the temporal growth rate ω_i for the S-mode with streamwise wavenumber k_x for different values of B ($B \leq 0.5$). (b) Variation of the temporal growth rate ω_i for the S-mode with streamwise wavenumber k_x for different values of B ($B \geq 1$).	61
3.13	(a) Variation of the neutral stability curve for the thermocapillary P-mode in (Re, k_x) plane for different values of B . (b) Variation of the temporal growth rate ω_i for the thermocapillary P-mode with streamwise wavenumber k_x for different values of B (top). Variation of the phase speed c_r for the thermocapillary P-mode with streamwise wavenumber k_x for different values of B (bottom).	62
3.14	(a) Variation of the neutral stability curve for the shear mode in (Re, k_x) plane for different values of the Biot number Bi . (b) Variation of the temporal growth rate ω_i for the shear mode with streamwise wavenumber k_x for different values of Bi	63

3.15	(a) Variation of the neutral stability curve for the H-mode and S-mode in (Re, k_x) plane for different values of the slip length β . (b) Variation of the temporal growth rate ω_i for the H-mode with streamwise wavenumber k_x for different values of β (top). Variation of the temporal growth rate ω_i for the H-mode with streamwise wavenumber k_x for different values of β (bottom). (c) Variation of the temporal growth rate ω_i for the S-mode with streamwise wavenumber k_x for different values of β (top). Variation of the temporal growth rate ω_i for the S-mode with streamwise wavenumber k_x for different values of β (bottom).	64
3.16	(a) Variation of the neutral stability curve for the thermocapillary P-mode in (Re, k_x) plane for different values of the slip length. (b) Variation of the temporal growth rate ω_i for the thermocapillary P-mode with streamwise wavenumber k_x for different values of β (top). Variation of the phase speed c_r for the thermocapillary P-mode with streamwise wavenumber k_x for different values of β (bottom).	66
3.17	(a) Variation of the neutral stability curve for the shear mode in (Re, k_x) plane for different values of the slip length β . (b) Variation of the temporal growth rate ω_i for the shear mode with streamwise wavenumber k_x for different values of β .	67
3.18	(a) Variation of the neutral stability curve for the thermocapillary P-mode in (Re, k_x) plane for different values of the Prandtl number. (b) Variation of the temporal growth rate ω_i for the thermocapillary P-mode with streamwise wavenumber k_x for different values of Pr (top). Variation of the phase speed c_r for the thermocapillary P-mode with streamwise wavenumber k_x for different values of Pr (bottom).	69
3.19	(a) Variation of the neutral stability curve for the H-mode and S-mode in (Re, k_x) plane for different values of the spanwise wavenumber and $M_T = 25$. (b) Variation of the neutral stability curve for the H-mode and S-mode in (Re, k_x) plane for different values of the spanwise wavenumber and $M_T = 30$.	70
3.20	(a) Variation of the neutral stability curve for the thermocapillary P-mode in (Re, k_x) plane for different values of the spanwise wavenumber. (b) Variation of the neutral stability curve for the shear mode in (Re, k_x) plane for different values of the spanwise wavenumber.	70
3.21	(a) Variation of the neutral stability curve for the H-mode in (k_x, k_z) plane for different values of the Reynolds number. (b) Variation of the neutral stability curve for the S-mode in (k_x, k_z) plane for different values of the Reynolds number. (c) Variation of the neutral stability curve for the P-mode in (k_x, k_z) plane for different values of the Reynolds number. (d) Variation of the neutral stability curve for the shear mode in (k_x, k_z) plane for different values of the Reynolds number.	72

4.1	Sketch of a viscous film flowing down a heated inclined plane in the presence of an imposed shear stress in the streamwise direction. . . .	74
4.2	(a) Variation of the critical thermal Marangoni number Ma_{Tc} with the Biot number Bi when the inclination angle θ alters. (b) Variation of the critical Reynolds number Re_c with the Biot number Bi	88
4.3	(a) Comparison of the neutral stability curve for the H-mode with the results computed from the Padé approximation and the numerical simulation in (Re, k_x) plane. (b) Comparison of the temporal growth rate for the H-mode with the results computed from the Padé approximation and the numerical simulation.	91
4.4	(a) Variation of the temporal growth rate ω_i for the H-mode with streamwise wavenumber k_x for different values of M_T . The solid points are the results of Ding <i>et al.</i> (b) Variation of the neutral stability curves in (k_x, G) plane for different values of M_T . The solid points are the results of Hu <i>et al.</i>	93
4.5	(a) Variation of the relative error E_N with the number of Chebyshev polynomials N for different values of M_T . (b) Variation of the relative error E_N with the number of Chebyshev polynomials N for different values of τ	96
4.6	(a)-(d) The eigenvalues in (c_r, c_i) plane for different unstable modes of instability.	97
4.7	(a) Variation of the neutral stability curves for the H-mode and the S-mode in (Re, k_x) plane for different values of the imposed shear stress $\tau \geq 0$. Variations of the onset of instability Re_c for the H-mode and the onset of stability Re_s for the S-mode are shown in the inset of Fig. 4.7(a). (b) Variation of the neutral stability curve for the P-mode in (Re, k_x) plane for different values of the imposed shear stress $\tau \geq 0$. Variations of the onset of instability Re_{pi} and the onset of stability Re_{ps} for the P-mode are shown in the inset of Fig. 4.7(b).	98
4.8	(a) Variation of the neutral stability curves for the H-mode and the S-mode in (Re, k_x) plane for different values of the imposed shear stress $\tau \leq 0$. Variations of the onset of instability Re_c for the H-mode and the onset of stability Re_s for the S-mode are shown in the inset of Fig. 4.8(a). (b) Variation of the neutral stability curve for the P-mode in (Re, k_x) plane for different values of the imposed shear stress $\tau < 0$. Variations of the onset of instability Re_{pi} and the onset of stability Re_{ps} for the P-mode are shown in the inset of Fig. 4.8(b). (c) The phase boundary for the existence of distinct unstable zones corresponding to the H-mode and S-mode.	101
4.9	(a) Variation of the neutral stability curves for the H-mode and S-mode in (Re, k_x) plane for different values of the spanwise wavenumber k_z . (b) Variation of the neutral stability curve for the P-mode in (Re, k_x) plane for different values of the spanwise wavenumber. . . .	102

4.10	(a) Variation of the neutral stability curve for the shear mode in (Re, k_x) plane for different values of the imposed shear stress $\tau(\geq 0)$. (b) Variation of the neutral stability curve for the shear mode in (Re, k_x) plane for different values of the imposed shear stress $\tau(\leq 0)$. Variation of the critical Reynolds number Re_i for the onset of instability corresponding to the shear mode is shown in the inset of Figs. 4.10(a) & 4.10(b), respectively.	104
4.11	(a) Variation of the neutral stability curves for the H-mode and the shear mode in (Re, k_x) plane for different values of the imposed shear stress τ . (b) Competition between the H-mode and the shear mode in (Re, k_x) plane. (c) The phase boundary for the distinct unstable zones corresponding to the H-mode and the shear mode.	105
4.12	Variation of the neutral stability curves for the H-mode and the shear mode in (Re, k_x) plane for different values of the spanwise wavenumber k_z	107
4.13	(a) Variation of the neutral stability curve for the inertialess instability in (Ma_T, k) plane for different values of the Biot number ($Bi \geq 1$). (b) Variation of the neutral stability curve for the inertialess instability in (Ma_T, k) plane for different values of the Biot number ($Bi \leq 1$). (c) Comparison of the neutral stability curve for the inertialess instability with the results computed from the Padé approximation and the long-wave solutions in (Ma_T, k) plane.	111
4.14	Sketch of spreading of a viscous film flowing down an inclined plane in the presence of an imposed shear stress in the streamwise direction.	116
5.1	A schematic diagram of a thin viscous liquid film falling down a uniformly heated inclined wall in the presence of a constant shear stress.	122
5.2	(a) Variation of the critical Reynolds number Re_{cs} for the H-mode when the imposed shear stress τ varies. (b) Schematic diagram of a physical mechanism for the H-mode instability. (c) Variation of $\frac{Ma_S}{Ma_T}$ with the Biot number Bi when τ changes.	135
5.3	(a) Comparison of the neutral stability curves in (Re, k) plane for the H-mode. (b) Comparison of the associated temporal growth rates in (k, ω_i) plane. (c) Comparison of the neutral stability curves in (Pe_S, k) plane for the surfactant mode. (d) Comparison of the associated temporal growth rates in (k, ω_i) plane.	141
5.4	(a) Variation of the neutral stability curve corresponding to the surfactant mode in (Pe_S, k) plane for different values of the thermal Marangoni number Ma_T . (b) The associated temporal growth rate in (k, ω_i) plane for different values of Ma_T . Solid points are the results of Bhat and Samanta.	142
5.5	(a)-(j) The eigenvalues in (c_r, c_i) plane and respective eigenfunctions for different unstable modes of instability.	147

5.6	(a) Variation of the neutral stability curves for the H-mode and S-mode in (Re, k) plane for different values of M_S . (b) Variation of the neutral stability curves for the H-mode and S-mode in (Re, k) plane for different values of M_T	148
5.7	(a) Variation of the neutral stability curve for the P-mode in (Re, k) plane for different values of M_S . (b) Variation of the neutral stability curve for the P-mode in (Re, k) plane for different values of M_T	150
5.8	(a) Variation of the neutral stability curve for the surfactant mode in (Pe_S, k) plane for different values of M_T when $M_S = 2.475$ as well as for different values of M_S . (b) Variation of the temporal growth rate ω_i for the surfactant mode with streamwise wavenumber k for different values of M_T when $Pe_S = 140$ and $M_S = 2.475$ as well as for different values of M_S . The solid points are the results of Bhat and Samanta.	152
5.9	(a) Variation of the neutral stability curve for the surfactant mode in (Pe_S, k) plane for different values of B ($B \leq 0.5$). (b) Variation of the temporal growth rate ω_i for the surfactant mode for different values of B . (c) Variation of the neutral stability curve for the surfactant mode in (Pe_S, k) plane for different values of B ($B \geq 0.5$). (d) Variation of the temporal growth rate ω_i for the surfactant mode for different values of B	153
5.10	(a) Variation of the neutral stability curve for the shear mode in (Re, k) plane for different values of the surfactant Marangoni number Ma_S . (b) Variation of the neutral stability curve for the shear mode in (Re, k) plane for different values of the thermal Marangoni number Ma_T	155
5.11	(a) Variation of the critical Reynolds number Re_c for the shear mode instability when the surfactant Marangoni number Ma_S and the thermal Marangoni number Ma_T vary. Star point represents data ($Ma_S = 2.5, Ma_T = 15$). The circular symbols in solid and dashed lines represent the data $Ma_S = 4.8$ and $Ma_T = 125$, respectively. (b) Variation of the neutral stability curve for the shear mode in (Re, k) plane.	157
5.12	(a) Variation of the neutral stability curve for the surfactant mode in (Pe_S, k) plane. (b) Variation of the neutral stability curve for the surfactant mode in (Pe_S, k) plane for different values of Ma_T . (c) Variation of the temporal growth rate ω_i with wavenumber k when Ma_T changes and $Pe_S = 150$. Thick lines represent the results with inertia ($Re = 80$) and thin lines represent the results without inertia ($Re = 0$).	162

List of Tables

3.1	Comparison between the analytical and numerical values of the critical Reynolds number Re_c for the H-mode when the parameter M_T varies.	51
4.1	List of different non-dimensional numbers and their expressions	78
4.2	Comparison between the analytical and numerical values of the critical Reynolds number Re_c for the H-mode when the imposed shear stress τ changes.	94
5.1	Comparison between the analytical and numerical values of the critical Reynolds number Re_{cs} for the H-mode (surface mode) when the surfactant Marangoni number Ma_S varies.	145
5.2	Comparison between the analytical and numerical values of the critical surfactant Péclet number Pe_{cm} for the surfactant mode when the surfactant Marangoni number Ma_S varies.	145

Symbols

Bi	Biot number
c_p	Specific heat capacity at constant pressure
c	Complex wave speed
d	Height of undisturbed film
Ca	Capillary number
D_s	Diffusivity of surfactant
g	Gravitational acceleration
h	Height of disturbed film
k	Total wavenumber
k_x	Streamwise wavenumber
k_z	Spanwise wavenumber
Ma_S	Surfactant Marangoni number
Ma_T	Thermal Marangoni number
p	Pressure field
P_a	Ambient pressure
Pe_S	Surfactant Peclet number
Pe_T	Thermal Peclet number
Pr	Prandtl number
P_n	n^{th} degree Chebyshev polynomial of first kind
Re	Reynolds number
t	Time
\bar{T}	Base flow temperature
\bar{U}	Base flow velocity
\mathbf{V}	Velocity vector
α	Dimensional slip length

β	Non-dimensional slip length
η	Non-dimensional amplitude of free surface deformation
λ	Heat transfer coefficient
μ	Dynamic viscosity
ν	Kinematic viscosity
ν	Thermal diffusivity
κ	Thermal conductivity
ρ	Density of fluid
σ	Surface tension
ψ	Non-dimensional stream-function
ϕ	Non-dimensional amplitude of stream-function
ω	Circular frequency
Γ	Surfactant concentration
$\boldsymbol{\tau}$	Stress tensor
τ_s	Imposed shear stress
θ	Angle of inclination